

On the Streakiness of Katabatic Wind Signatures on High-Resolution AVHRR Satellite Images: Results from the Aircraft-Based Experiment KABEG

By Günther Heinemann¹

Abstract: Signatures of the katabatic wind on high-resolution satellite imagery can often be detected as streaks in the infrared brightness temperatures. The relation to the katabatic wind system is commonly thought to be caused by a wind pattern in the boundary layer, which leads to spatial variations of the snow drift intensity, thus influencing the temperature of the emitting surface and the emissivity. Data of the aircraft-based experiment KABEG'97 (Katabatic wind and boundary layer front experiment around Greenland) performed in April/May 1997 are used to study the characteristics of these thermal streaks and their relation to boundary layer structures in detail. For katabatic wind flights during different synoptic situations and surface conditions with low-level jets with wind speeds up to 25 m/s the surface temperature patterns were found to agree with those found in the AVHRR data. Snow drift can be ruled out to be the primary reason for the streaks, and a connection to the surface topography was found instead. The katabatic streaks seem to be a signal of the surface inversion strength being related to the wind speed.

Zusammenfassung: In hochaufgelösten Satellitenbildern findet man häufig Signaturen des katabatischen Windes in Form von streifenförmigen Mustern der Infrarot-Strahlungstemperatur. Als Verbindung zum katabatischen Windsystem wird i.a. ein entsprechendes Muster des Windfeldes in der Grenzschicht angenommen, das zu räumlichen Variationen der Schneedrift-Intensität führt, die wiederum die Temperatur der emittierenden Oberfläche und die Emissivität beeinflusst. Messungen des flugzeuggestützten Experiments KABEG'97 (Katabatic wind and boundary layer front experiment around Greenland), das im April/Mai 1997 durchgeführt wurde, werden zur detaillierten Untersuchung dieser thermischen Streifenmuster ("katabatic streaks") und ihrer Beziehung zu Grenzschichtstrukturen verwendet. Für Flüge im katabatischen Windsystem mit "Low-Level-Jets" von bis zu 25 m/s Windstärke bei unterschiedlichen synoptischen Situationen und Oberflächenbedingungen werden Muster der Oberflächentemperatur gefunden, die mit denen der AVHRR-Daten übereinstimmen. Schneedrift kann als primäre Ursache für die "katabatic streaks" ausgeschlossen werden, dagegen wird eine Verbindung mit Topographiestrukturen gefunden. Die "katabatic streaks" sind demnach ein Signal der Stärke der Bodeninversion in Abhängigkeit von der Windstärke.

INTRODUCTION

The near-surface wind field over the large ice sheets of the Antarctic and Greenland is dominated by katabatic winds in the stably-stratified boundary layer. Apart from their role in the exchange of energy and momentum between the atmosphere and the underlying surface, katabatic-driven near-surface winds are important for field workers and scientific or logistic aircraft missions, since wind speeds may rise up to gale force (PUTNINS 1970, BALL 1960, WENDLER 1990, HEINEMANN 1999). The East

Greenland "piteraq" events, which represent strong synoptically enforced katabatic winds, are well-known to the Inuits and weather forecasters in Greenland (RASMUSSEN 1989).

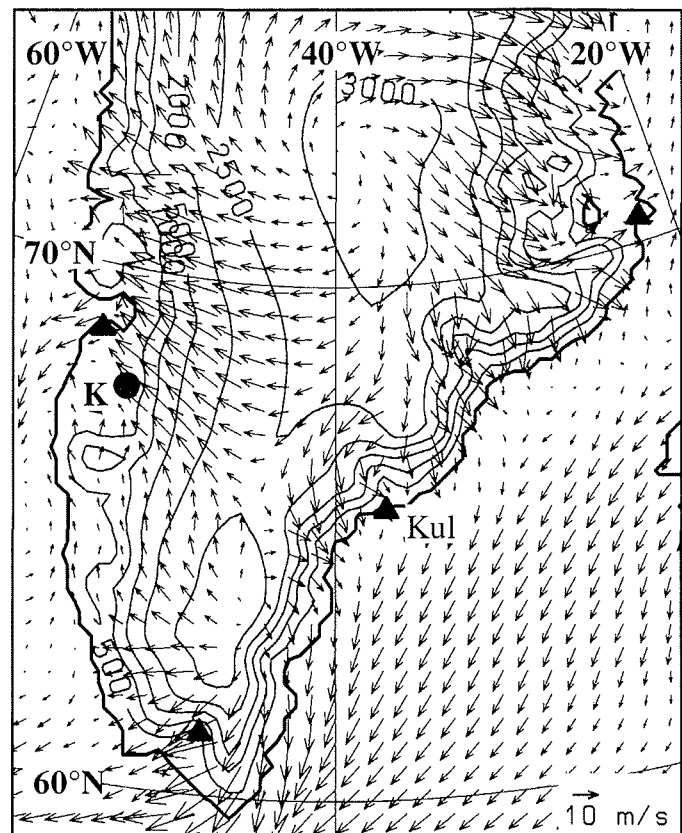


Fig.1: Topography (full lines, isolines 500 m) and NORLAM simulation of the near-surface wind (10 m above the surface) for South Greenland after 24 h simulation valid for 22 April 1997, 0600 UTC. Triangles mark radiosonde stations (Kul = Kulusuk), K = location of Kangerlussuaq. Grid resolution is 25 km, but only every second wind vector is shown (scaling vector in the lower right corner).

Abb. 1: Topographie (durchgezogene Linien, Isolinienabstand 500 m) und die NORLAM-Simulation des oberflächennahen Windes (10 m über der Oberfläche) für Südgrönland nach 24 h Simulation gültig für den 22. April 1997, 0600 UTC. Dreiecke markieren Radiosondenstationen (Kul = Kulusuk), "K" zeigt die Position von Kangerlussuaq. Die Gitterauflösung ist 25 km, es wird nur jeder zweite Windvektor gezeigt (Skalierungsvektor unten rechts).

¹ Meteorologisches Institut der Universität Bonn, Auf dem Hügel 20, D-53121 Bonn, Germany, gheinemann@uni-bonn.de.

A relatively good description of the katabatic-driven near-surface wind can be given by three-dimensional simulations with

meso-scale models (e.g. BROMWICH et al. 1996, HEINEMANN 1996). An example of a numerical simulation of the katabatic wind regime for Greenland is shown in Figure 1 for 0600 UTC, 22 April 1997. The numerical simulation was performed with the meso-scale weather forecast model NORLAM (Norwegian Limited Area Model) as described in HEINEMANN (1997). The model was started at 0000 UTC 21 April 1997 with analyses of the European Centre for Medium-Range Weather Forecasting (ECMWF), which were also taken as boundary conditions for a NORLAM run with 50 km horizontal resolution (LAM50). A NORLAM model with 25 km horizontal resolution and 40 vertical sigma levels (LAM 25) was nested into the LAM50 grid. The 30 hours simulation of LAM25 for wind vector at the lowest sigma level (10 m above the ground) is shown in Figure 1. The katabatic wind system is fully developed at that time. The dominant influence of the topography structure on the near-surface wind field is obvious. While a fairly homogeneous wind field with wind speeds around 15 m/s is found over West Greenland, channeling effects are present in areas of coastal valleys in East Greenland. Very pronounced channeling effects occur near Kulusuk/Tasiilaq (Angmagssalik) at the coast of East Greenland, where the above mentioned "piteraq" occur.

RASMUSSEN (1989) observed signatures of the katabatic wind on Advanced Very High-Resolution Radiometer (AVHRR) satellite imagery. The infrared images of the full resolution AVHRR data (1.1 km resolution) often show streak patterns over the ice sheet, which extend over more than 100 km length. An example is given in Figure 2 for 6 UTC, 22 April 1997, i.e. at the same time as the NORLAM simulations (Fig. 1). The streaks are aligned to the expected flow lines of the katabatic wind, and even confluence zones in the valleys at the east coast of Greenland are depicted well by the streaks (see Fig. 1). This observational evidence is used by RASMUSSEN (1989) to construct a katabatic flow pattern over Greenland using the streak patterns from AVHRR imagery. He proposes that meso-scale circulations similar to roll clouds during convective cold air outbreaks cause spatial variations of the snow drift intensity, thus influencing the temperature of the emitting surface and the emissivity. Although the mechanism of elongated roll-like circulations in the stable boundary layer remains unclear, this would have important consequences for nowcasting katabatic winds over the sloped ice sheet, where only very few observations are available. The intensity and orientation of the infrared streaks would then represent a direct observational signal for the intensity and direction of the near-surface wind. In the present paper, this question is investigated using AVHRR data and aircraft data of the experiment KABEG'97 (Katabatic wind and boundary layer front experiment around Greenland), which was performed in April/May 1997 in the area of southern Greenland (HEINEMANN 1998, HEINEMANN 1999). KABEG was a cooperative project of the Meteorological Institute University of Bonn (MIUB) and the Alfred Wegener Institute for Polar and Marine Research (AWI, Bremerhaven).



Fig.2: High-resolution (1.1 km) AVHRR infrared image of South Greenland for 22 April 1997, 0600 UTC.

Abb. 2: Hochaufgelöstes (1.1 km) AVHRR-Infrarot-Bild von Südgrönland für den 22. April 1997, 0600 UTC.

DATA

Detailed measurements were carried out during the KABEG experiment from mid of April to mid of May 1997. The research aircraft POLAR2 owned by AWI was based at Kangerlussuaq (former Søndre Strømfjord, West Greenland) at a distance of about 20 km from the glaciers of the inland ice sheet. Kangerlussuaq was selected as the base in order to investigate (a) the development of the katabatic flow over relatively homogeneous topography under different synoptic conditions and (b) the mod-

Quantity	Sampling in Hz	Measurement system, instrument
<u>METEOPOD</u>		
Air temperature	120	PT100 open wire (Rosemount)
Air temperature	120	PT100 open wire (AWI)
Air humidity	120	Lyman- α (AIR)
Air humidity	12	Humicap, PT100 in Rosemount housing (Aerodata)
Air humidity	12	Dew point mirror (Gen. Eastern)
Air pressure	12	Pressure sensor (Rosemount)
3D wind vector	120	5-hole probe (Rosemount)
Acceleration	60	Attitude and Heading Reference System LTR81 (Litton)
Height	120	Radar altimeter (TRT)
<u>BASIC INSTRUMENTATION</u>		
Acceleration	60	LaserNav Inertial Platform Navigation (Honeywell)
Height	12	Radar altimeter
Position	12	GPS (SEL)
Surface temperature	12	KT4 (Heimann), 8-14 mm, 0.6° opening angle
Downward and	12	Short wave: pyranometer (Eppley)
Upward radiometer	12	Long wave: pyrgeometer (Eppley)
<u>fluxes</u>		
<u>ADDITIONAL INSTRUMENTATION</u>		
Height	500	Laser altimeter (Ibeo)

Tab. 1: POLAR2 instrumentation during KABEG.

Tab. 1: Instrumentierung der POLAR2 während KABEG.

ification of the katabatic flow in the transition zone ice/tundra. The research aircraft POLAR2 was instrumented with the turbulence measuring device "METEOPD", allowing high-resolution measurements of turbulent momentum, sensible and latent heat fluxes (Tab. 1). In addition, downward and upward solar and terrestrial radiation and surface temperature were measured; a high-resolution laser altimeter registered surface roughness structures. During the experiment, several surface stations were installed, including direct turbulent heat flux and momentum measurements, surface layer profile and surface energy balance measurements over the ice sheet and the tundra area (for details see HEINEMANN 1999).

Full resolution AVHRR data for the KABEG period were obtained from the High-Resolution Picture Transmission (HRPT) data receiving station at Kangerlussuaq (operated by the Danish Meteorological Institute), but for the KABEG period part of the data was lost because of a malfunction of the magneto-optical disk device. Fortunately, HRPT data with a nadir resolution of 1.1 km were provided by the Canadian Weather Service for most of the flight missions. Digital raw data were processed at MIUB. Only infrared data are used here.

The present paper aims to demonstrate that small-scale topography structures of the ice surface are related to the observed katabatic streaks. For Greenland, a topography data set with a

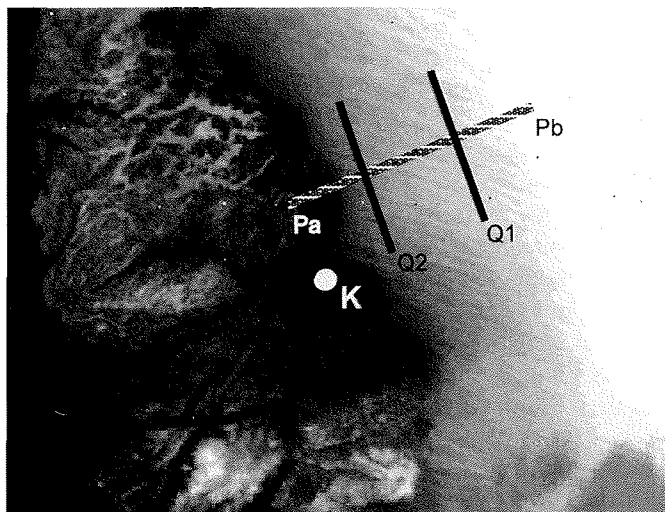


Fig.3a: High-resolution AVHRR infrared images of the Kangerlussuaq area (K = Kangerlussuaq).

22 April 1997, 0600 UTC, with the main flight tracks of the KABEG aircraft superimposed (Pa-Pb is the along-slope leg, Q1 and Q2 are the two across-slope legs).

Abb. 3a: Hochaufgelöste AVHRR-Infrarot-Bilder der Region Kangerlussuaq ("K" markiert Kangerlussuaq). Teil a: 22. April 1997, 0600 UTC, die Haupt-Flugwege der KABEG-Flugzeugmessungen sind überlagert (Pa-Pb ist das Leg entlang des Hangs, Q1 und Q2 sind zwei Quer-Legs).

resolution of about 2 km is available (EKHOLM 1996). This

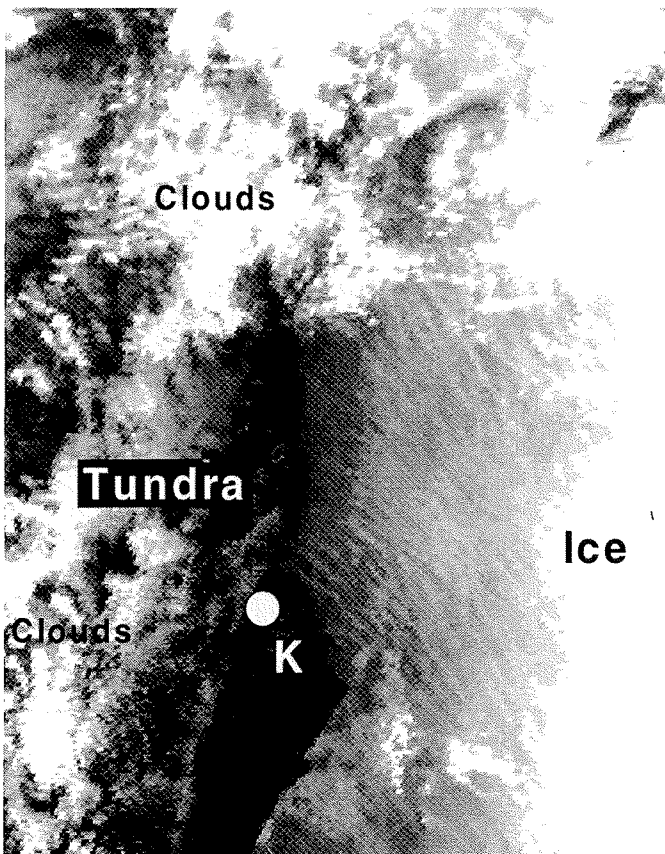
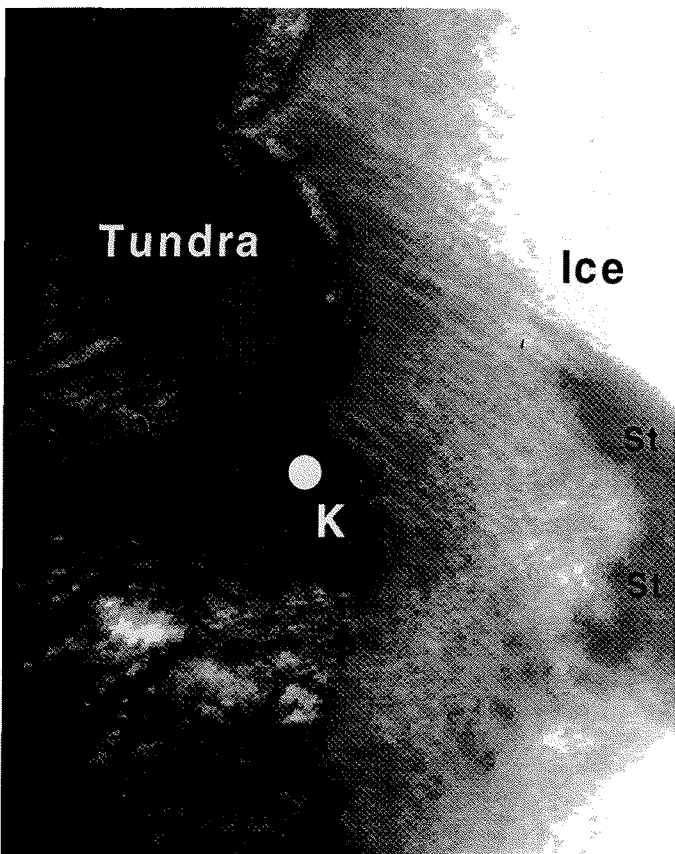


Fig. 3b and c: High-resolution AVHRR infrared images of the Kangerlussuaq area (K = Kangerlussuaq). (b): 21 April 1997, 0600 UTC ("St" marks low stratus clouds). (c): 18 April 1997, 0600 UTC.

Abb. 3b und c: Hochaufgelöste AVHRR-Infrarot-Bilder der Region Kangerlussuaq ("K" markiert Kangerlussuaq). Teil b: 21. April 1997, 0600 UTC ("St" markiert tiefe stratiforme Wolken). Teil c: 18. April 1997, 0600 UTC.

Greenland digital elevation model was constructed from GEOSAT and ERS-1 satellite altimetry, airborne radar and laser altimetry, and stereo photogrammetry scannings.

From the KABEG aircraft measurements the elevation of the ice surface (above sea level) was also derived in the following way: high-precision pressure data of the aircraft were first used to compute a barometric height. Independent height data relative to the surface were measured by two radars (METEOPD, 120 Hz, and basic aircraft instrumentation, 12 Hz) as well as by the laser altimeter (500 Hz). Since for a comparison with satellite data such a high resolution is not needed, only 1 Hz sampled data from the METEOPD radar were used (horizontal resolution of about 70 m). The difference between barometric height and radar height represents an aircraft-derived surface elevation above sea level (referred to as aircraft-derived topography hereafter). An offset to the absolute topography can be expected, because horizontal pressure gradients and the time dependence of the pressure field were not considered. But, as will be demonstrated below, the topography structure can be derived with good accuracy using the aircraft data.

KATABATIC STREAK OBSERVATIONS DURING KABEG

A typical katabatic streak image during the KABEG period is shown in Figure 3a (a subsection of Fig. 2) for an area of West Greenland for 0600 UTC, 22 April 1997. The infrared AVHRR image shows the typical streaks with temperature variations of about 1 °C and a cross-slope wavelength of about 10 km. This small horizontal scale is also responsible for the fact, that katabatic wind streaks are invisible on AVHRR images with lower resolution, that is the Global Area Coverage (GAC) data with a reduced resolution of 4 km (nadir) archived at NOAA/NESDIS. The streaks do not extend over the tundra area, which is in agreement with the aircraft investigation of the katabatic wind extent for this area (HEINEMANN 1999). Streak signatures like that shown in Figure 3a were observed on all days during the KABEG experiment being favourable for the katabatic wind development, i.e. a high pressure system over Greenland with no clouds or only few high clouds. Additional examples are given in Figures 3b and 3c for the area of Kangerlussuaq. The image for 0600 UTC, 21 April 1997 (Fig. 3b) shows a small area of low stratus (St) over the ice, but the area with katabatic streaks west and north of it is completely cloud-free. On 0600 UTC, 18 April 1997 (Fig. 3c) the tundra is mainly cloud-covered, but most of the ice area is cloud-free and the streak signature is again well developed.

Aircraft data of the KABEG flights over the ice sheet are available for eight different days simultaneously with AVHRR data (Tab. 2). The radiometric measurements of the surface temperature from low flight heights can be compared with the satellite brightness temperatures. The detailed meteorological aircraft data (high-resolution data of temperature, humidity and three-dimensional wind vector) and the observations by the mission scientist on board the aircraft allow to proof the thesis of RASMUSSEN (1989), i.e. if the streaks are a signal of a boundary layer

circulation with organized patterns of snow drift. The evaluation is restricted to the area near Kangerlussuaq, where six aircraft flights were performed on the flight pattern shown in Figure 3a (Tab. 2).

Date Time in UTC	Flight	Area
18 April 1997 0700-1145	KA1	Kangerlussuaq
21 April 1997 0630-1150	KA2	Kangerlussuaq
22 April 1997 0705-1210	KA3	Kangerlussuaq
29 April 1997 1020-1540	KA4	Kangerlussuaq
02 May 1997 0605-1150	KA5	Kangerlussuaq
11 May 1997 0635-1130	KA6	Kulusuk
11 May 1997 1300-1740	KA7	Kulusuk
13 May 1997 0600-1205	KA8	Kangerlussuaq
14 May 1997 0600-1135	KA9	Ilulissat

Tab. 2: Aircraft flights for the KABEG katabatic wind program.

Tab. 2: Messflüge des katabatischen Windes während KABEG.

Before discussing the streak problem, the main findings about the katabatic wind system from the KABEG data will be briefly reviewed (a more detailed discussion is given in HEINEMANN 1999). Data of the KABEG surface stations along the line Pa-Pb in Figure 3a show a pronounced daily cycle of the near-surface wind for almost all days due to the nighttime development of the katabatic wind. Generally, the wind speed maximum occurred during the early morning hours. Vertical profiles flown by the aircraft ("temps") yielded boundary layer heights over the ice slope between 70 and 200 m, and low-level jets (LLJs) with wind speeds of up to 25 m/s. Studies of the boundary layer dynamics yielded the results that the katabatic flow was always shooting (Froude numbers >1) and that the katabatic force is the main driving mechanism for the flow regime, but the synoptic forcing is also significant.

As an example for the katabatic wind structure, Figure 4 shows vertical profiles of an aircraft temp in the centre of Q1 (see Fig. 3a) for 0901 UTC 21 April 1997, which is about 3 hours later than the corresponding satellite image in Figure 3b. The profiles

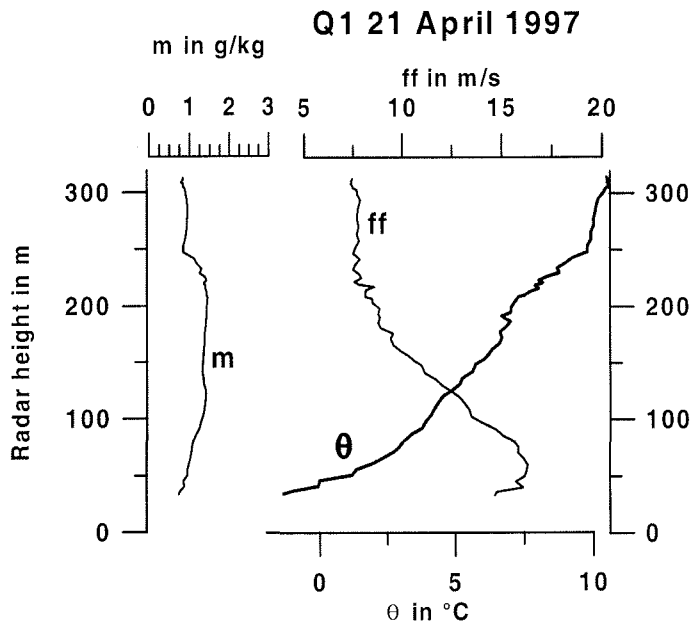


Fig.4: Aircraft temp at 0901 UTC 21 April in the centre of the Q1 leg (see Fig. 3a) showing the profiles of the mixing ratio (m), potential temperature (q), and wind speed (ff).

Abb. 4: Flugzeugtemp um 09.01 UTC am 21. April in der Mitte des Legs Q1 (siehe Abb.3a) mit den Profilen des Mischungsverhältnisses (m), der potentiellen Temperatur (θ) und der Windstärke (ff).

are plotted against the METEOPD radar height (i.e. above the surface). The lowest point for the profile corresponds to a barometric height of about 1450 m. A pronounced surface inversion of about 6K/150m is present in the lowest 200 m. A LLJ at a height of 60-90 m with wind speeds of more than 15 m/s is found in the stable boundary layer. The mixing ratio and the potential temperature indicate a boundary layer height of about 250 m. The wind speed in the free atmosphere is only 7.5 m/s.

The surface potential temperature (θ_s , computed from the aircraft-measured radiometric surface temperature) and the aircraft-derived topography from a low-level flight (30 m) along the flight leg Q1 (see Fig. 3a) between 0914 and 0930 UTC on 21 April are displayed in Figure 5. AVHRR brightness temperatures along Q1 for 0600 UTC are also shown. Like on the satellite image (Fig. 3b), pronounced temperature variations with an amplitude of about 1 °C and a horizontal distance of 3-8 km are found in the aircraft data. The major signatures of the aircraft-measured θ_s agree with those found in the AVHRR data for 0600 UTC. Variations on the same horizontal scale as in the surface temperature are present in the aircraft-derived topography. The ice topography, which seems to have a completely flat and homogeneous structure at a first glance, reveals undular height changes of up to 20-40 m. The comparison to the surface temperature data yields positive correlations for several anomalies with "valleys" being associated with colder temperatures, but also differences, which seem to be a result of a phase shift between the topography and the θ_s structures. The topography data of the EKHOLOM (1996) data set, interpolated to the Q1 leg, shows much smoother structures, particularly no pronounced variations on the katabatic streak scale.

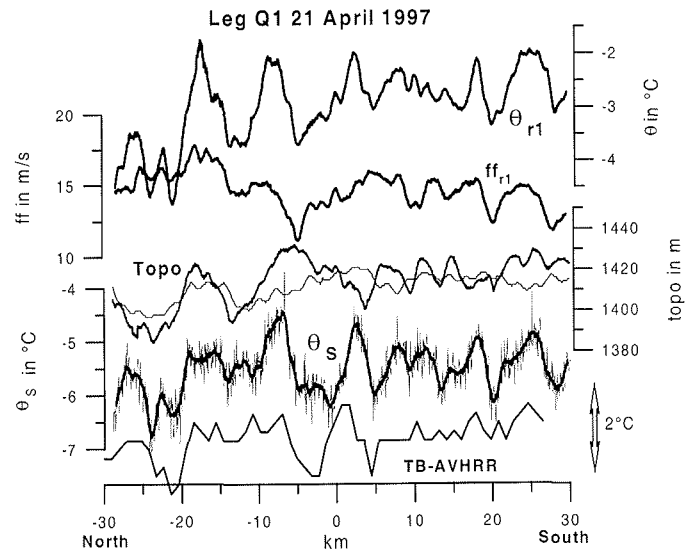


Fig.5: Aircraft data along Q1 from a low-level flight leg (about 30 m) between 0914 and 0930 UTC on 21 April 1997. AVHRR brightness temperatures (TB-AVHRR) along Q1 for 6 UTC are also shown (2 °C scale on the right). 1 Hz data (thin line) and a running mean (window of about 850 m, thick line) are shown for the radiometric surface potential temperature (θ_s). Aircraft-derived topography (thick line, 1 Hz data) is shown together with topography data of the EKHOLOM (1996) data set, interpolated to the Q1 leg (thin line). The air potential temperature (θ) and wind speed (ff) are shown as running means (window of about 850 m) and are adjusted to a reference height of 30 m (see text).

Abb. 5: Flugzeugmessungen entlang Q1 in der untersten Flughöhe (ca. 30 m über Grund) im Zeitraum 09.14 und 09.30 UTC am 21. April 1997. AVHRR-Strahlungstemperaturen (TB-AVHRR) entlang Q1 für 06 UTC sind ebenfalls dargestellt (2 °C Skala rechts). 1 Hz Daten (dünne Linie) und das gleitende Mittel (Fensterbreite ca. 850 m, dicke Linie) werden gezeigt für die potentielle Oberflächentemperatur (θ_s) aus Flugzeug-Radiometermessungen. Die aus den Flugzeugmessungen abgeleitete Topographie (dicke Linie, 1 Hz Daten) ist zusammen mit den auf das Leg Q1 interpolierten Topographie-Daten nach EKHOLOM (1996) dargestellt (dünne Linie). Die höhenadjustierte potentielle Temperatur der Luft θ_r und Windstärke ff_r werden als gleitende Mittel (Fensterbreite ca. 850 m) gezeigt (adjustiert bezüglich einer Referenzhöhe von 30 m, s. Text).

The same findings were made during other flights. While for the case shown above intense snow drift was observed (in accordance with Rasmussen's thesis), the same temperature signal was also found for a flight without snow drift and weaker wind speeds. For the case of 18 April, 0600 UTC, shown in Figure 3c, a low-level jet of about 15 m/s was measured at 100 m above the ground, and wind speeds at 2 m measured by the surface stations on the ice were about 7 m/s. Despite the fact that no snow drift was observed during the flight on 18 April, the streak signature is as strong as for situations with intense snow drift (Fig. 3a and 3b). Therefore, the flight observations can reject the thesis that elongated roll circulations in the katabatic wind layer are directly responsible for emissivity or temperature changes due to the snow drift. On the other hand, the aircraft data showed the (unexpected) topography structures on the scale of the satellite-observed brightness temperature observations for every flight.

Across-slope topographic structures

The flight pattern Q1 was flown during six flights in the Kangerlussuaq area either in form of constant level legs (on 18, 21 and

29 April) and/or in form of aircraft temps (18, 21, 22, and 29 April, 2 May and 13 May). Figure 6 summarizes the aircraft-derived topography along Q1 for four different flights. Since the aircraft was navigated by GPS, the spatial differences for different days were relatively small. The deviation in distance from the line Q1 was only about 500 m in general. However, on 18 April and 13 May deviations of up to 2 km occur for some parts of the flight leg, which results in larger differences to the topography cross-sections (not shown in Fig. 6). Apart from a bias caused by the different horizontal pressure gradients for the different days, the data in Figure 6 show a remarkable consistent

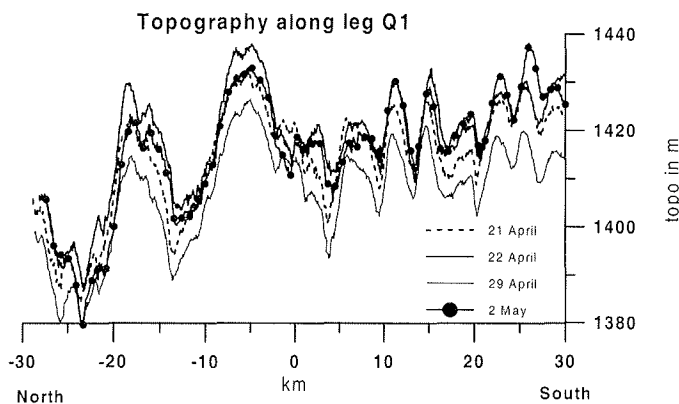


Fig.6: Aircraft-derived topography for the Q1 leg for 21, 22 and 29 April and 2 May 1997.

Abb. 6: Aus Flugzeugmessungen abgeleitete Topographie für das Q1-Leg für den 21., 22. und 29. April sowie den 2. Mai 1997.

variation of topography along Q1. Only minor differences can be seen in the topography derived from constant flight legs (21 and 29 April) or from aircraft temps (22 April and 2 May). The same finding cannot be expected for the radiometric surface temperature, since an air mass of about 300 m thickness (the difference between the highest and the lowest altitude of an aircraft temp along Q1) can contribute significantly to the observed signal of 1-2 °C. A direct comparison of the θ_s pattern along Q1 for constant level leg and the temps on 21 April (which were flown within 30 min) yielded differences of up to 0.5 °C, but the same gross structures. On the other hand, information about a possible roll circulation cannot be obtained from the temps. Since the flight on 29 April was much later than the other flights (in order to investigate the dissipating katabatic wind system), only a weak θ_s variation was found. This is consistent with the fact that the corresponding AVHRR images did not show katabatic wind streaks either. In the following, the relationship between θ_s , the low-level potential temperature and wind speed along Q1 will be discussed for 21 April.

The observed θ_s /topography correlation is not valid everywhere (see Fig. 5) and is also different for different flights. This may be explained by the three-dimensional nature of the interaction between the katabatic flow and the topography structures. Since the direction of the near-surface katabatic flow with respect to the topography anomalies varies depending on the synoptic sit-

uation, a flow modification must occur which is also dependent on the pre-history of the flow when regarding a single cross-section as in Figure 5, although the topography structures remain unchanged. The signatures of the θ_s anomalies are also reflected by the air temperature at the lowest flight level on 21 April (Fig. 5). Since height variations of the aircraft relative to the ground have a large effect on the temperature and wind data in the very stable surface layer (see Fig. 4), the potential temperature of the air (θ) shown in Figure 5 was adjusted to a reference height of 30 m using a linear regression between θ and the radar height for the leg Q1. In addition, the data were smoothed using a running average of about 850 m in order to filter small-scale turbulence. A good correlation exists between θ_s and θ . The wind speed (adjusted in the same way as the temperature) also shows large variations along the leg Q1 (ranging from 11 to 18 m/s). The complex interaction between topography, wind speed and temperature can be seen e.g. for the "hill" between 0 and -10 km horizontal coordinate, where a temperature increase with increasing topography is observed in the left part, while the drop in wind speed leads to a temperature drop in the right part.

Along-slope topographic structures

The flight pattern Pa-Pb (see Fig. 3a) was flown several times during each flight. Most of the flight legs were constant level legs at different heights. Because of the strong topography gradient along Pa-Pb, the analysis must be different compared to Q1. Although the data set of EKHOLOM (1996) does not contain the relevant small-scale topography structures, it can be used to derive a reference height data set for the larger-scale structures along the slope. For this purpose, the Ekholm topography profile along Pa-Pb has been approximated over the ice by a logarithmic fit:

$$Z_{\text{fit}} = -579.29 + 473.184 \cdot \log(x) \quad (1)$$

x (in km) is the horizontal coordinate (being zero at Pa, and the inland ice edge at $x = 16$ km), Z_{fit} (in m) is the approximated ice surface elevation. The accuracy of this fit describing the Ekholm topography over the ice ($x > 16$ km) is surprisingly good with a correlation of 0.9994 and a standard deviation of about 25 m. From the so defined analytical and smooth reference topography given by (1) the difference to the actual, aircraft-derived topography can be computed (dtopo). Figure 7 summarizes the aircraft-derived dtopo (from the lowest flight level) along the slope over the ice for all flights (except for 18 April, where the deviation from Pa-Pb was much larger than for the other flights). As already seen in the discussion of the Q1 topography, the ice slope is far from being smooth on a scale of a few kilometers. In the first 30 kilometers (up to a topographic height of about 1250 m), a rather irregular structure is present, while higher up-slope more regular variations with the same scale as the Q1 cross-section can be found (100 km along-slope coordinate corresponds to a topographic height of about 1600 m). Again, the topography structures remain unchanged for the whole measuring period.

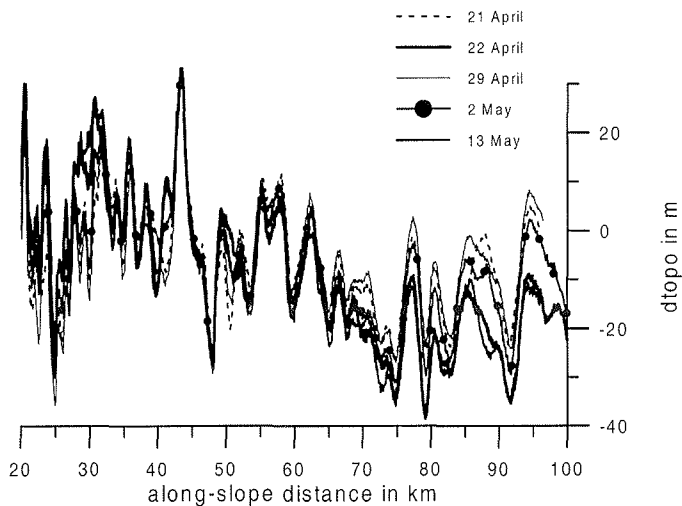


Fig.7: Aircraft-derived topography deviation (dtopo) from the fit of Equation (1) for the P leg (line Pa-Pb) for 21, 22 and 29 April, and 2 and 13 May 1997.

Abb. 7: Aus Flugzeugmessungen abgeleitete Topographie-Anomalie (dtopo) von der Näherung nach Gleichung (1) für das P-Leg (Linie Pa-Pb) für den 21., 22. und 29. April, sowie für den 2. und 13. Mai 1997.

The $\theta/dtopo$ correlation for the Pa-Pb leg is as complex as for Q1. The signatures of the θ_s anomalies have again a length scale of about 10 km and are also reflected by the temperature at 30 m above the surface for 22 April (Fig. 8). As for Q1, the potential temperatures of the air shown in Figure 8 were adjusted to reference heights of 30, 60 and 90 m, respectively, using a linear regression between θ and the radar height over the ice. While unsmoothed data are also plotted for dtopo and θ_s , the data at 100, 200 and 300 ft were smoothed using a running average of about 850 m. A good correlation exists between θ_s and $\theta(30\text{ m})$,

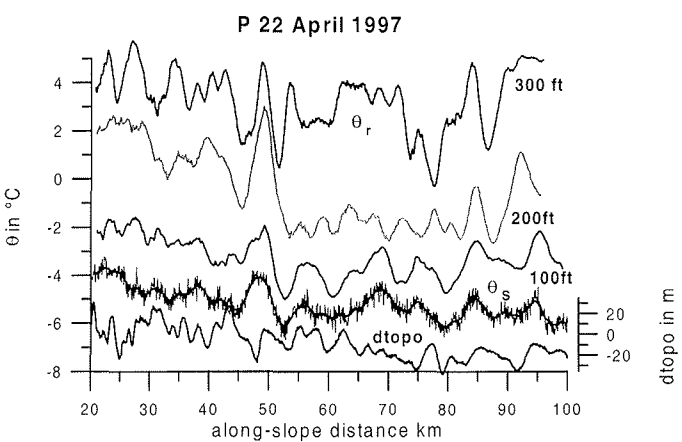


Fig.8: Aircraft data along Pa-Pb for 22 April. 1 Hz data and a running mean (window of about 850 m) are shown for the radiometric surface potential temperature (θ_s). Only running means are shown for the aircraft-derived topography deviation (dtopo) and air potential temperatures at 100ft/30m, 200ft/60m and 300ft/90m (temperatures adjusted to corresponding reference heights, see text).

Abb. 8: Flugzeugmessungen entlang Pa-Pb für den 22. April. 1 Hz Daten und das gleitende Mittel (Fensterbreite ca. 850 m, dicke Linie) werden gezeigt für die potentielle Oberflächentemperatur (θ_s) aus Flugzeug-Radiometermessungen. Die aus Flugzeugmessungen abgeleitete Topographie-Anomalie (dtopo) und höhenadjustierte potentielle Temperaturen der Luft werden als gleitende Mittel gezeigt (adjustiert bezüglich der Referenzhöhen 100 ft / 30m, 200 ft / 60 m und 300 ft / 90 m, siehe Text).

at higher levels signals can be seen associated with θ_s peaks at 50 and 85 km along-slope coordinate. The "topography anomaly" dtopo shows again no unique relation to θ_s due to the complex interaction between topography anomaly, wind speed and temperature.

SPECTRAL AND CORRELATION ANALYSIS

In order to get more insight into the scale and correlation of different aircraft-measured quantities, auto- and cross-correlation analyses as well as power-spectrum analyses were performed. As an example, the powerspectra for Q1 on 21 April for the topography (topo), θ_s , the height-corrected air temperature θ_{r1} and wind speed ff_{r1} of the lowest flight level (corrected to a reference height of 30 m, see above) are displayed in Figure 9. The spectra show broad maxima in the low-frequency part (around $6-8 \cdot 10^{-3}$ Hz), but also weak maxima in the high-frequency part (around $3-4 \cdot 10^{-1}$ Hz). The frequencies can be converted to wavelengths using the ground speed of the aircraft, which is 60 m/s for this case. For the atmospheric quantities the high-frequency maximum has a wavelength of about 200 m and is related to processes of the scale of the boundary layer height, while the low-frequency maxima have scales of about 10 km. A second maximum is present for the topography at about $2 \cdot 10^{-2}$ Hz or 3 km. In order to prevent correlations related to small-scale turbulence, a low-pass filtering of the data was performed using a cut-off of 40 s, that is a frequency of $2.5 \cdot 10^{-2}$ or a wavelength of about 2.5 km.

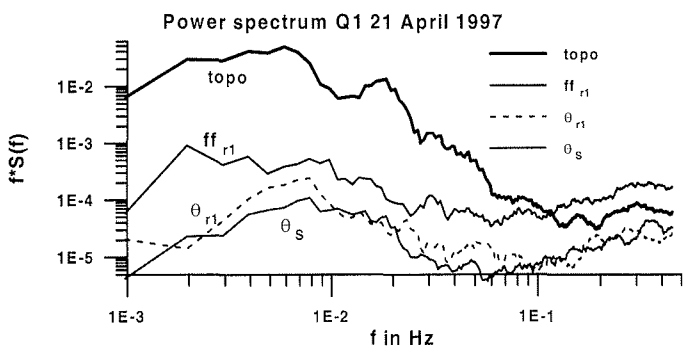


Fig.9: Power spectra for topography (topo), wind speed (ff_{r1}), surface potential temperature (θ_s) and air potential temperature (θ_{r1}) for aircraft data along Q1 from a low-level flight leg (temperatures and wind speed adjusted to a reference height of 30 m) between 0914 and 0930 UTC on 21 April 1997.

Abb. 9: Power-Spektren für die Topographie (topo), Windstärke (ff_{r1}), potentielle Oberflächentemperatur (θ_s) und potentielle Temperatur der Luft (θ_{r1}) für Flugzeugmessungen entlang Q1 (Temperaturen und Windstärke adjustiert bezüglich einer Referenzhöhe von 30 m) im Zeitraum 09.14 und 09.30 UTC am 21. April 1997.

The auto- and cross-correlation analyses agree with those of the powerspectrum analyses. Table 3 summarizes the results of the cross-correlation analyses of the topography and θ_s for Q1 for all flight days. The correlation coefficient is highly variable, and secondary maxima around a lag of 13 km are found. Typical values for the standard deviations (STDV) are 9 m for topography and 0.4 K for temperatures. The temperature signal is weak for 29 April, 2 and 13 May.

Date	STDV		$r_{ab}(0)$	L2/ $r_{ab}(L2)$
	Q_s	Topo		
18 April	0.4 K	7.2 m	0.17	13/0.33
21 April	0.4 K	9.0 m	0.39	12/0.43
22 April	0.3 K	8.9 m	0.14	15/0.46
29 April	0.2 K	8.4 m	0.46	
02 May	0.2 K	8.6 m	0.05	13/0.35
13 May	0.2 K	8.7 m	0.25	16/0.62

Tab. 3: Standard deviations (STDV), crosscorrelations (r_{ab}) at lag 0 and secondary maxima at lag L2 (in km, if exceeding $r_{ab}(0)$) for the flight leg Q1 for the aircraft-derived topography (topo) and the aircraft-measured surface potential temperature (Θ_s). Data are low-pass filtered using a cut-off of 40 s (wavelength of about 2.5 km).

Tab. 3: Standardabweichungen (STDV) und Kreuzkorrelationen (r_{ab}) bei einer Verschiebung von 0 und sekundäre Maxima bei einer Verschiebung L2 (in km, falls größer als $r_{ab}(0)$) für das Flugleg Q1 für die aus den Flugzeugmessungen abgeleitete Topographie (topo) und die potentielle Oberflächentemperatur (Θ_s) aus Flugzeug-Radiometermessungen. Die Daten wurden tiefpass-gefiltert mit einem Cut-off von 40 s (ca. 2.5 km Wellenlänge).

A further cross-correlation analysis of atmospheric variables (Tab. 4) is presented for Q1 on 21 April and for all flights on the P leg (Pa-Pb, only data between 20 and 100 km coordinate, i.e. only over the ice). The flight of 18 January was excluded, since the lowest flight level was sometimes above the LLJ, and cross-correlations differ completely from the other flights with a higher LLJ. The wind speed has relatively high STDV values (0.7-1.1 m/s), and temperature STDVs are slightly higher on the P leg compared to the Q1 leg (see Tab. 3). The focus of this analysis is the coupling between the wind speed and the surface temperature as well as the internal coupling between wind speed and air temperature. In general the correlations are higher compared to Table 3. Highest cross-correlations are present between Θ_s and air temperatures (up to 0.82), indicating the good surface/air coupling in the lowest part of the boundary layer. The internal coupling between air temperature and wind speed is also relatively high (exceeding 0.7 for 29 April and 2 May), but a contribution of an inadequate height correction cannot be ruled out. Of particular interest is the correlation between wind speed and Θ_s , which shows areas with high winds being related to high Θ_s . Again, large variations exist between different days. It can be concluded that the relation of spatial structures of atmospheric quantities to the topography along the flight track is depending on the direction of the katabatic flow, which in turn depends on the synoptic-scale forcing (see HEINEMANN 1999). The advective effects associated with the undular ice surface structures found in the aircraft data are different for each flight, and represent a coupling between the atmospheric conditions on a flight leg with the upstream (unknown) topography. This high variation of correlations between different days was found also for the coupling between the (local) topography gradient and the wind speed on the P legs (not shown). In contrast, the internal

correlation between atmospheric quantities and between wind speed and surface temperature is generally much higher.

Date	a	STDV _a	b	STDV _b	$r_{ab}(0)$
Leg					
21 April Q1	Θ_s	0.4 K	ff_{r1}	1.1 ms ⁻¹	0.21
	Θ_s	0.4 K	Θ_{r1}	0.5 K	0.81
	ff_{r1}	1.1 ms ⁻¹	Θ_{r1}	0.5 K	0.40
21 April P	Θ_s	0.6 K	ff_{r1}	0.7 ms ⁻¹	0.33
	Θ_s	0.6 K	Θ_{r1}	0.7 K	0.52
	ff_{r1}	0.7 ms ⁻¹	Θ_{r1}	0.7 K	0.44
22 April P	Θ_s	0.4 K	ff_{r1}	0.9 ms ⁻¹	0.59
	Θ_s	0.4 K	Θ_{r1}	0.7 K	0.77
	ff_{r1}	0.9 ms ⁻¹	Θ_{r1}	0.7 K	0.42
29 April P	Θ_s	0.3 K	ff_{r1}	0.8 ms ⁻¹	0.66
	Θ_s	0.3 K	Θ_{r1}	0.2 K	0.71
	ff_{r1}	0.8 ms ⁻¹	Θ_{r1}	0.2 K	0.74
02 May P	Θ_s	0.4 K	ff_{r1}	0.7 ms ⁻¹	0.53
	Θ_s	0.4 K	Θ_{r1}	0.6 K	0.65
	ff_{r1}	0.7 ms ⁻¹	Θ_{r1}	0.6 K	0.43
13 May P	Θ_s	0.3 K	ff_{r1}	1.1 ms ⁻¹	0.47
	Θ_s	0.3 K	Θ_{r1}	0.5 K	0.82
	ff_{r1}	1.1 ms ⁻¹	Θ_{r1}	0.5 K	0.72

Tab. 4: Standard deviations (STDV) and crosscorrelations (r_{ab}) at lag 0 for the following quantities: aircraft-measured surface potential temperature (Θ_s), height-corrected air temperature Θ_{r1} and wind speed ff_{r1} of the lowest flight level (corrected to a reference height of 30 m). Data are low-pass filtered using a cut-off of 40 s (wavelength of about 2.5 km).

Tab. 4: Standardabweichungen (STDV) und Kreuzkorrelationen (r_{ab}) bei einer Verschiebung von 0 für die folgenden Größen: potentielle Oberflächentemperatur (Θ_s) aus Flugzeug-Radiometermessungen, höhenadjustierte potentielle Temperatur der Luft Θ_{r1} und Windstärke ff_{r1} im untersten Flugniveau (adjustiert bezüglich einer Referenzhöhe von 30 m). Die Daten wurden tiefpass-gefiltert mit einem Cut-off von 40 s (ca. 2.5 km Wellenlänge).

DISCUSSION

Aircraft altimetry has been used to derive high-resolution ice topography data along the flight patterns of the KABEG experiment. Undular topography structures with a 10-20 m height change over a distance of 10 km were found (ice undulations). Over a period of about four weeks between the first and the last flight, these undulations remained almost unchanged, indicating that they represent a long-term signal. The reasons for the observed undular topography structures are not clear. The currently available high-resolution (2.2 km) topography data set of EKHOLM (1996) does not contain these structures (plotted in Fig. 5 for comparison). Topography structures derived by SAR interferometry data for other regions of West Greenland (BINDSCHADLER 1998) seem to agree with the scale of the topography anomalies found during KABEG. Concerning the katabatic wind

streaks observed on high-resolution AVHRR imagery, the new thesis from the KABEG results is the following:

Katabatic streaks are associated with topography anomalies. The observed katabatic streak signal in the AVHRR data is therefore not correlated with the katabatic wind intensity, but with the strength of the surface inversion. Since the formation of a surface inversion is a precondition for the katabatic wind development, a link to the presence of the katabatic wind is given, but strong katabatic winds can also reduce the inversion strength via increased mixing.

A number of questions arise from this thesis. The first question is about the geometric shape of the topography anomalies. A simple correlation between the infrared streak signal and topography would require long (100-200 km) elongated topography structures approximately aligned to the katabatic wind. In a recent publication (TOMLIN 1999) evidence is shown for the existence of elongated snow structures in the Antarctic (megadunes of more than 100 km length), which could explain katabatic streaks, if they would be oriented along the mean wind direction. But, these megadunes seem to be oriented perpendicular to the katabatic wind in Antarctica. The common feature to the ice undulations is the persistence over long time periods (several decades for the Antarctic megadunes). The available information from SAR interferometry (BINDSCHADLER 1998) as well as the KABEG data do not show this kind of topography structures, but a hilly structure instead. Detailed topography maps in the ablation zone of the Greenlandic ice sheet also show lakes in regular distances of about 10 km in some areas (OHMURA, pers. comm.). This is also evident in the digital ERS-1 SAR mosaic of the Greenland ice sheet published by National Snow and Ice Data Center (NSIDC). Figure 10 shows the SAR subsection for the KABEG measurement area near Kangerlussuaq. In the left side of the picture is the tundra area, in the middle is the ablation zone with small lakes on the ice and ice undulations with separation distances of several kilometres. In the right part of the image there are some "SAR streaks", which have the same direction as the thermal AVHRR streaks, and extend over tens of kilometres. The SAR data for the Kangerlussuaq area, which were obtained after the main melting season during August of 1992, therefore give further evidence for the ice undulations on the same scale as found during KABEG.

A second question is the origin of the topography anomalies. Surface undulations on moving ice caps are well-known to glaciologists (HUTTER 1983). Surface waves on the ice with dominant wavelengths of several times the ice thickness can develop because of bedrock inhomogeneities, but also because of sudden changes in the accumulation rates. These "shallow ice waves" can travel at speeds much larger than the ice flow (HUTTER 1983). It seems to be reasonable that the observed ice undulations are a result of the ice flow dynamics, but a long-term forcing of the mean katabatic flow could also contribute to the formation of the topography anomalies by spatially varying snow accumulation. The SAR streaks over the higher ice elevations may be related to meltwater drainage paths that are oriented along elongated ridges parallel to the mean surface wind.

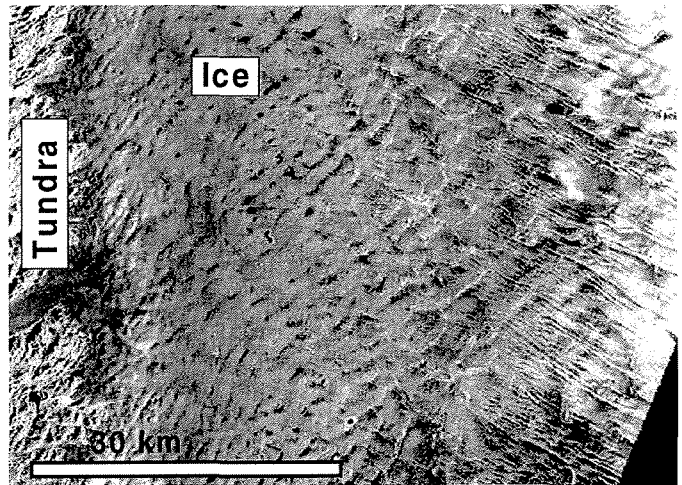


Fig.10: Digital ERS-1 SAR image of the Greenland ice sheet from data published by NSIDC (1997) for the subsection for the KABEG measurement area near Kangerlussuaq.

Abb. 10: Digitales ERS-1 SAR-Bild des grönländischen Eisschildes aus Daten von NSIDC (1997) für das KABEG-Messgebiet nahe Kangerlussuaq.

This would partly revive Rasmussen's thesis of snow drift and an associated secondary circulation, but on a different time scale and in a more indirect role. The coupling between the aircraft-measured larger-scale wind and temperature patterns supports this thesis. But, despite of the high accuracy of the aircraft data, it is not possible to measure reliable vertical winds on this scale in order to derive the structure of a possible secondary circulation.

Assuming that the ice dynamics generate a more or less regular pattern of undulations on the ice surface, a simple conceptual model of the katabatic wind streaks can be derived. The idea is that the katabatic wind is locally enhanced/decreased in areas where the topography gradient is increased/decreased by the undulations on the sloped ice surface. Figure 11a shows an idealized ice topography, where the topography fit of the KABEG area given by Equation (1) was assumed to be homogeneous along the y-axis, and a two-dimensional harmonic undulation was superimposed (amplitude 10 m, wavelengths 8 km). The katabatic flow caused by a sloped inversion over the ice can be described using the integrated momentum equations (BALL 1956):

$$\frac{d\mathbf{V}_m}{dt} = -\frac{1}{\rho_m} \nabla p - f \mathbf{k} \times \mathbf{V}_m - \frac{1}{\rho_m h} \boldsymbol{\tau}(z_s) \quad (2)$$

\mathbf{V}_m is the horizontal wind vector tangential to the slope and ρ_m is the air density (the index m indicates the mean over the katabatic wind layer of height h). The forces on the right hand side are the two-dimensional pressure gradient force, the Coriolis force ($f = \text{Coriolis parameter}$) and friction ($\boldsymbol{\tau}(z_s)$ is the surface momentum flux vector). Setting the left side to zero (stationary, no advection), rotating the y-axis parallel to the pressure gradient, and assuming a bulk formulation for the surface momentum flux vector results in:

$$0 = f \cdot v_m - \frac{C_D}{h} \cdot |V_m| \cdot u_m \quad (3)$$

$$0 = F - f \cdot u_m - \frac{C_D}{h} \cdot |V_m| \cdot v_m$$

F is the absolute value of the pressure gradient force, and C_D the bulk exchange coefficient for momentum. Equations (3) can be solved analytically. F is described by the pure katabatic pressure gradient force caused by an inversion being parallel to the slope (BALL 1956):

$$F = g \frac{\Delta\theta_m}{\theta_m} \alpha \quad (4)$$

α is the local slope, $\Delta\theta_m$ the inversion strength, and θ_m the mean potential temperature. This results in a balanced wind field depending only on the local topography gradient, if the inversion strength is horizontally homogeneous (e.g. BALL 1960, PARISH & BROMWICH 1986). The application of this simple model to the topography of Figure 11a would result in a similar pattern for the wind field, with wind directions being approximately 45° from the local fall line. As advective/inertia effects cannot be neglected, this simple Ball model was modified by assuming a downstream propagation (exponentially damped) of the locally generated winds. Figure 11b shows the results for the wind speed using $C_D = 10^{-3}$, $\Delta\theta_m = 5$ K and $h = 100$ m. The advective effects smear out the areas of high winds in the direction of the flow, and a pattern similar to the observed katabatic streaks can be seen. The enhanced mixing in areas of increased wind speeds would result in warmer surface temperatures, so that the dark wind streaks in Figure 11b would correspond to dark signals in the infrared satellite image. It has to be pointed out that this conceptual model is not a realistic representation of the katabatic wind streak dynamics, since a regular pattern of the ice undulations and a simple approach for advective effects is assumed. On the other hand, it can give some hints for the explanation of the streak signature in the surface temperature, if the ice undulations are distributed quasi-regularly in a statistical sense. Since realistic high-quality ice sheet topographies with horizontal resolutions better than 1 km are presently not available, realistic streak simulations using more realistic three-dimensional atmospheric models are not possible.

Another interesting question is, if katabatic streaks are found also over Antarctica. In the southern hemisphere, the katabatic flow lines deviate to the left from the fall line, and strong katabatic winds are found in the coastal areas. As mentioned above, persistent Antarctic megadunes were recently found (TOMLIN 1999), and a relation to near-surface winds is assumed by glaciologists (SCAMBOS, pers. comm.), but there seems to be no connection to the streaks in the Antarctic, since the megadunes appear to be oriented perpendicular to the katabatic wind. While katabatic streaks on high-resolution AVHRR images have been often observed over Greenland, to the author's knowledge no comparable finding has been published for the Antarctic. Instead, many satellite studies show warm signatures associated

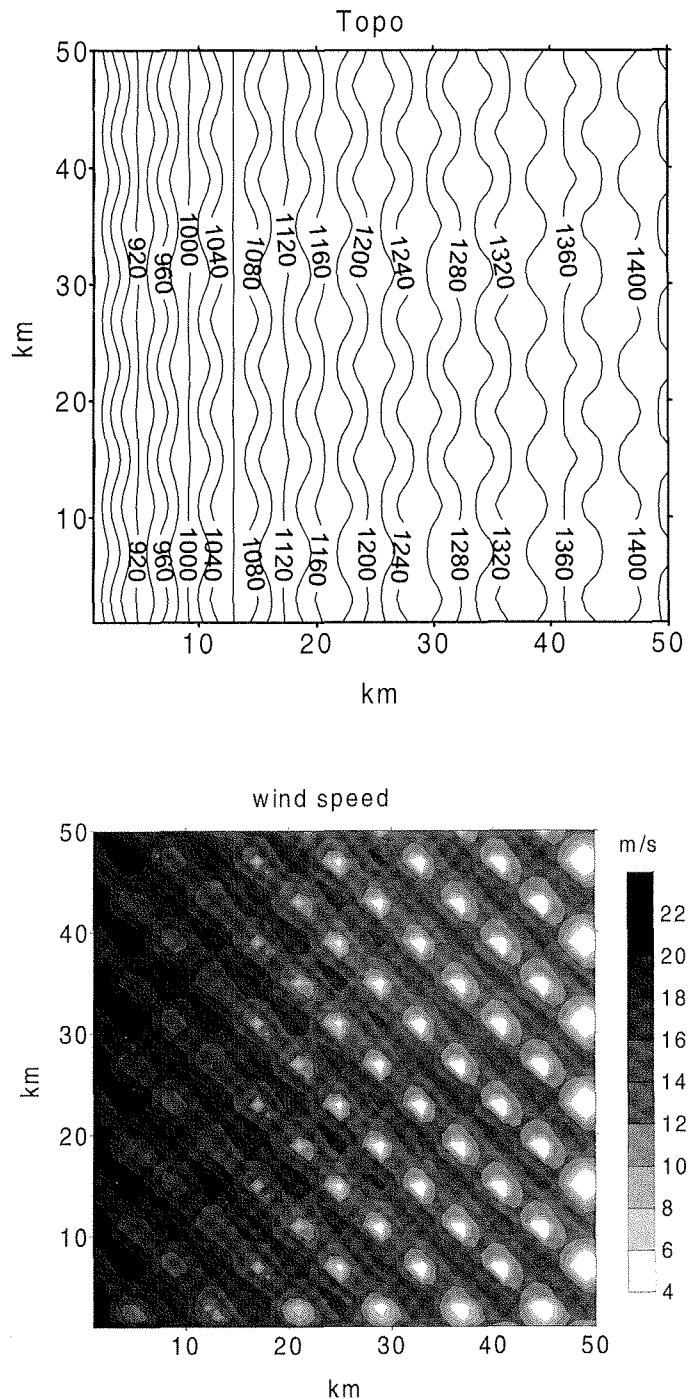


Fig.11: Part a: Idealized topography (isolines every 20 m) used in the conceptual model. topography. The fit of the KABEG area given by Equation (1) was assumed to be homogeneous along the y-axis, and a two-dimensional harmonic undulation was superimposed (amplitude 10 m, wavelengths 8 km). Part b: Wind speed pattern (gray shaded) of the modified Ball model resulting from the idealized topography shown in Fig. 11a. Darker areas correspond to higher wind speeds and warmer surface temperatures (see text).

Abb. 11: Teil a: Idealisierte Topographie (Isolinienabstand 20 m) für das konzeptionelle Modell. Die Topographie für das KABEG-Gebiet nach Gleichung (1) wird als homogen entlang der y-Achse angenommen, es ist eine zweidimensionale harmonische Schwingung überlagert (Amplitude 10 m, Wellenlängen 8 km). Teil b: Feld der Windstärke (grauschattiert) aus dem modifizierten Ball-Modell mit der idealisierten Topographie nach Abb. 11a. Dunklere Gebiete entsprechen höheren Windstärken und wärmeren Oberflächentemperaturen (siehe Text).

with katabatic surges in confluence zones (e.g. BROMWICH 1989). Summertime studies by the author for several years for the Weddell Sea area of Antarctica using satellite imagery with 2 km resolution have not shown any katabatic streaks. For southern hemisphere winter months only few sets of high-resolution AVHRR data are available to the author. One of the very few cases of Antarctic katabatic streaks is given in Figure 12 for the area of the West Antarctic. The high-resolution NOAA infrared image for 5 July 1994, 1500 UTC, shows two katabatic surges and an area of katabatic streaks over the steep slopes of Marie Byrd Land. The two surges are found in pronounced valleys, while the streaks are located over the more homogeneous parts of the slope. The streaks have the same horizontal scale as the Greenlandic ones, but deviate to the left from the fall line, which is in accordance with the reversed sign of the Coriolis parameter. The streaks shown in Figure 12 therefore appear to be parallel to the katabatic wind direction as it is the case for Greenland. The average slope in the area of the streaks can be estimated to be about 2 % (i.e. similar to Greenland), since the margin of the cold (white) plateau area corresponds to the 2000 m isoline and the ice shelf areas are close to sea level.

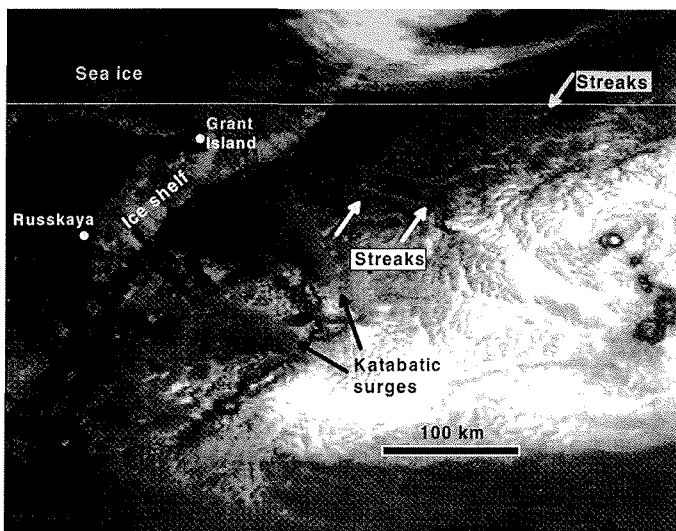


Fig.12: High-resolution AVHRR infrared image on 5 July 1994, 1500 UTC, for the area of Marie Byrd Land, West Antarctica. Two katabatic surges and the streak area are marked.

Abb. 12: Hochaufgelöstes (1.1 km) AVHRR Infrarot-Bild für den 5. Juli 1994, 1500 UTC, für das Gebiet von Marie Byrd Land, West-Antarktis. Zwei "katabatic surges" und ein Gebiet mit "katabatic streaks" sind gekennzeichnet.

Overall, the streak signal of Figure 12 is weaker compared to the Greenland cases, and is only observed in some regions. In contrast, streaks could be found all around Greenland and on almost every cloud-free night during KABEG (see Fig.2). A reason may be that in Antarctica no melting occurs even during summer, while melting rates are quite high over the Greenlandic slopes. It can be speculated, to what extent the katabatic wind and the ice dynamics influenced by the melting phase can contribute to ice forms.

SUMMARY

Signatures of the katabatic wind on high-resolution satellite imagery can often be detected as streaks in the infrared brightness temperatures. Infrared images of the full resolution AVHRR (1.1 km resolution) show these streak patterns as dark parallel lines over the ice sheet extending over more than 100 km length and having horizontal distances of about 10 km. The streaks are aligned to the expected flow lines of the katabatic wind, and have been used by RASMUSSEN (1989) to construct a katabatic flow pattern over Greenland. The physical reasons for the infrared signal can be spatial variations of the physical temperature of the emitting surface and the emissivity. The mechanism for the streaks proposed by RASMUSSEN (1989) is that elongated roll-like circulations in the stable boundary layer produce snow drift patterns, and thereby emissivity and surface temperature patterns.

AVHRR data and aircraft data of the experiment KABEG'97 performed in April/May 1997 in the area of southern Greenland (HEINEMANN 1998, 1999) are used to study the characteristics of these thermal streaks and their relation to boundary layer structures in detail. Emissivity variations associated with snow drift can be ruled out to be responsible for the temperature streaks, but a connection to the surface topography and the wind speed was found instead. Aircraft altimetry has been used to derive high-resolution ice topography data along the flight patterns of the KABEG experiment. Undular topography structures (ice undulations) with a 10-20 m height change over a distance of about 10 km were found. A simple conceptual model based on the integrated model of BALL (1956) could explain the existence of the streaks, if the ice undulations are distributed quasi-regularly. High-resolution simulations using more realistic three-dimensional atmospheric models are desirable at least for idealized topographies. Because of the unavailability of high-quality ice sheet topographies with horizontal resolutions better than 1 km, realistic streak simulations will be not possible in the near future.

It is not within the scope of the paper to answer the question about the origin of the topography anomalies, their structure and dynamics. The possible interaction between katabatic winds, melting and accumulation, and surface waves on the ice could be an interesting part of interdisciplinary research between glaciologists and meteorologists.

ACKNOWLEDGMENTS

AVHRR data have been provided by the DMI (Kangerlussuaq) and by the Canadian Weather Service. KABEG is supported by the Bundesministerium für Bildung und Forschung under grant BMBF-03PL020F, and by the Deutsche Forschungsgemeinschaft under grant He2740/1. The aircraft program was funded by AWI. Thanks go also to T. Klein from MIUB for providing Figure 1.

References

- Ball, F.K.* (1956): The theory of strong katabatic winds.- *Aust. J. Phys.* 9: 373-386.
- Ball, F.K.* (1960): Winds on the ice slopes of Antarctica.- *Proc. Sympos. Antarctic Meteorology*, Pergamon Press: 9-16.
- Bromwich, D.H.* (1989): Satellite analyses of Antarctic katabatic wind behaviour.- *Bull. Amer. Meteor. Soc.* 70: 738-749.
- Bromwich, D.H., Du, Y., Hines, K.M.* (1996): Wintertime surface winds over the Greenland ice sheet.- *Mon. Wea. Rev.* 124: 1941-1947.
- Ekholm, S.* (1996): A full coverage, high-resolution, topographic model of Greenland computed from a variety of digital elevation data.- *J. Geophys. Res.* 101: 21961-21972.
- Heinemann, G.* (1996): Katabatic wind systems over polar ice sheets.- In: *Proceedings 6th Workshop on mass balance of the Greenland ice sheet and related topics*, 22-23 January 1996, Copenhagen, Denmark. *The Geol. Surv. Greenland Report* 53: 39-43.
- Heinemann, G.* (1997): Idealized simulations of the Antarctic katabatic wind system with a three-dimensional meso-scale model.- *J. Geophys. Res.* 102: 13825-13834.
- Heinemann, G.* (1998): Katabatic wind and boundary layer front experiment around Greenland (KABEG) field phase report.- *Rep. Polar Res.* 269, 93 pp.
- Heinemann, G.* (1999): The KABEG'97 field experiment: An aircraft-based study of the katabatic wind dynamics over the Greenlandic ice sheet.- *Boundary Layer Meteorol.* 93: 75-116.
- Hutter, K.* (1983): *Theoretical glaciology*. D. Reidel Publ. Co., Dordrecht, Holland, 510 pp.
- NSIDC* (1997): *Digital SAR Mosaic and Elevation Map of the Greenland Ice Sheet, Version 1.0.*- National Snow and Ice Data Center, Univ. Colorado, Boulder, USA.
- Parish, T.R., & Bromwich, D.H.* (1986): The inversion wind pattern over West Antarctica.- *Mon. Wea. Rev.* 114: 849-860.
- Punins, P.* (1970): The climate of Greenland.- In: *S. ORVIG (ed.), Climates of the polar regions*, *World Survey Climatol.* 14: 3-113.
- Rasmussen, L.* (1989): Greenland winds and satellite imagery.- *Vejret, Danish Meteorol. Soc.*: 32-37.
- Tomlin, S.* (1999): Vast snow dunes frozen in time.- *Nature* 402: 860.
- Wendler, G.* (1990): Strong gravity flow observed along the slope of eastern Antarctica.- *Meteorol. Atmos. Phys.* 43: 127-135.